Chapter 18

In Situ Metal-Free Synthesis of Polylactide Enantiomers Grafted from Nanoclays of High Thermostability

Giada Lo Re,* Philippe Dubois, and Jean-Marie Raquez

**Center of Innovation and Research in Materials and Polymers (CIRMAP),
University of Mons - UMONS, Place du Parc 23, 7000 Mons, Belgium**
E-mail: giada.lore@umons.ac.be.

Renewable origin, controlled synthesis, good mechanical properties, and inherent biocompatibility make Polylactide (PLA) the most interesting renewable polymers for broad applications. For this reason, several strategies are carried out to span the range of applications for PLA and overcome its intrinsic drawbacks such as a low crystallization rate, thermal resistance and the use of metal-based catalysis for its synthesis. Adding nanosized fillers are among them the most studied and applied approach to enhance the performance of PLA-based materials. In order to achieve an enhanced interfacial adhesion and fine filler dispersion with the surrounding matrix, *in situ* polymerization constitutes the most viable and promising way to overcome this issue. In addition, stereocomplexation as well as organocatalysis make part of the emerging challenges to further improve the performance and extend the range of applications of the PLA-based materials such as in biomedical realm.

In this chapter, the metal-free synthesis of enantiomeric PLA/clay nanohybrids through ring-opening polymerization (ROP) of lactide is investigated, with the aim to produce stereocomplexed bionanocomposites with enhanced thermal properties. Different techniques to quench the polymerization reaction were thereby studied in order to overcome the main drawback related to the organocatalysis used for ROP of

lactide, *i.e.*, by causing intensive degradation on further melt-processing. Stereocomplexed polylactide/nanoclays bionanocomposites were prepared and their related thermal properties were investigated.

Introduction

Polylactide (PLA) is one of the most interesting and useful renewable and biodegradable polymers because of its renewable origin, biodegradability, controlled synthesis, good mechanical properties, and inherent biocompatibility (*1–5*) . However, PLA suffers from some drawbacks such as a low rigidity, slow crystallization rate and poor thermal-resistance. Moreover, the residual traces of metal-catalyst, mostly employed for its synthesis, limit its use in special applications such as the microelectronics or biomedical applications (*6*).

The literature reports several strategies in order to span the range of applications for PLA, more particularly by adding nanosized fillers, and the stereocomplexation. Nowadays, the metal-free synthesis of polylactide represents a new challenge to extend the use of PLA in the added-value market of microelectronic and biomedical applications (*7*).

Stereocomplexation is used to enhance the mechanical properties, the thermal-resistance, and the hydrolysis-resistance of PLA-based materials. Upon favorable thermodynamical parameters, in fact, an equivalent mixture of PLA of L-configuration (PLLA) and PLA of D-configuration (PDLA) forms a stereocomplex. Due to the strong Van der Waals interactions within the stereocomplex crystalline structure (*8–10*), melting temperature (T_m) of stereocomplexes can achieve a value above 220°C, which is approximately 50°C higher than T_m of either isotactic PLLA or PDLA (*11*).

Thermal, mechanical, rheological, barrier and other specific properties of the biopolymers can be improved by the incorporation of nanofillers. Blending renewable polymers with nanoparticles can yield a new class of hybrid materials, commonly known as bionanocomposites where the dispersed constituent has at least one dimension in the nanoscale size range. The nanosized dimensions of nanofillers enable their use in small quantities (weight percentage of 5-6%) into the polymer matrix. Improved thermal, mechanical and transport properties of PLA are often obtained via melt-blending layered silicate with the polylactide matrix in order to obtain bio-nanocomposites with enhanced performance (*12–18*). These improved properties are generally reached at low silicate content (less than 5 wt. %), due to the nanosized dimensions of the layered silicate. Using adequately organomodified nanoclay, specifically Cloisite 30B (Cl30B), intercalation of PLA chains into silicate galleries and even clay exfoliation throughout the polyester matrix are achieved (*19–21*). In the present work, the stereocomplexation and the addition of layered silicate nanofillers were investigated to cooperatively enhance the thermal properties and the crystallinity of PLA-based nanocomposites. Moreover, the "grafting from" approach was selected as a powerful tool for the enhancement of affinity between nanofillers and the matrix (*12, 22, 23*).

Nevertheless, the surface chemistry, specific surface area and volume effect of the nanofillers govern their common interactions, as well as the affinity towards the polymer matrix. These parameters, together with the size, the shape and the concentration, affect the extent of the nanofiller dispersion into the matrix. The large surface areas and low percolation thresholds as well as the availability and low cost make nanoclays the most used nanoparticles for polylactide, which attracted both industrial and academic interests. Indeed, several fields of applications such as medicine, textiles, cosmetics, agriculture, food-packaging, aerospace, construction, catalysis, and so on are expected from these bionanocomposites to substitute their petroleum-based counterparts.

Among the several methods adopted to improve the affinity between the polymeric matrix and the nanoclay, the *in-situ* polymerization of lactide, is a successful approach because of its flexibility in the synthetic parameters to tune the chain length and density on the filler surface, the improved dispersion of the filler in the matrix and related enhanced compatibility between the inorganic-organic phases. In particular, when the interactions between the filler and the polymer are of covalent bonding nature, the grafting achieved is generally combined to high performances for the resulting nanocomposites. In this respect "grafting from" methods, carrying out ring-opening polymerization of lactide through hydroxyl moieties from the quaternary ammoniums used for surface-treatment of nanoclays is preferred (*23*). As an example, PLA chains can be grafted at the surface of Cloisite®30B (CL30B), nanoclay organomodified in the presence of bis-2 hydroxyethyl, quaternary ammonium. CL30B was selected as model system among the most used, low cost and available commercial clays, due to the presence of "OH" end-group which can be used as initiator site for the ROP of lactide. In order to "graft" PLA chain from a clay surface, ROP of lactide (LA) is generally carried out in the presence of transition metal-based catalysts such as tin (II) octoate (*24*).

To avoid the current use of organometallic catalysts, we have recently reported the synthesis of PLLA and PDLA stereoisomers as directly grafted at the surface of CL30B via metal-free ROP of lactide carried out in chloroform at room temperature. To promote these reaction pathways in this work, 1,8-Diazabicyclo [5,4,0] undec-7-ene (DBU) was used as metal-free catalysts due to its excellent ability to control the polymerization of lactide at high yield (*25–27*). Although they exhibit several features such as low toxicity and compatibility, these metal-free catalysts have a high propensity to promote intensive side-reactions such as transesterification reactions at relatively high temperature and in the absence of solvent (*28*). An effective removal of the catalyst is therefore mandatory in order to obtain melt-processable PLA-based nanocomposites with improved performance. Some of us have reported that when DBU is used, a simple quenching reaction by using an excess of acid (forming the corresponding salt) followed by the precipitation of the polymer, can afford an effective way to obtain thermostable PLA (*28*). However, when stereocomplexed PLA are concerned, processing temperatures are so high, i.e., above 220°C, making these methods unsuccessful. In this chapter, current knowledge about *in situ* polymerization of polylactide from nanoclay by ROP achievements are used to prepare new bionanohybrids of clay-PLA metal free, pointing out different catalytic removal

methods. In addition to the quenching method using an excess of acid, a new route to quench the catalyst activity was investigated using the ion-exchange resin, to prepare the nanohybrids CL30B-graft-PLLA and CL30B-graft-PDLA (CL30B-*g*-PL(D)LA). The effectiveness of catalyst removal methods was assessed by the FTIR and DSC analysis on resulting nanohybrids. From the best quenching method, these nanohybrids were subsequently melt-processed together and with commercial PLA in order to elaborate stereocomplexed bionanocomposites with significantly improved thermal properties.

Experimental

Synthetic Approach

Commercial clay (CL30B, supplied by Southern Clay Products, USA), was introduced into a conditioned two-neck flask and dried under vacuum overnight. Meanwhile, L-lactide was hot-recrystallized. Briefly, L-lactide (supplied by Futerro) was dissolved in dry toluene, under stirring for 1 hour at 80 °C. Solution was put in a freezer to selectively precipitate the L-lactide monomer. The toluene was then removed from the flask by using a capillary and following by a drying step under vacuum at room temperature overnight. All products were stored in a glove box, in order to carry out the polymerization reaction under nitrogen atmosphere. Thereby, L-lactide and dried CL30B were solubilized in dry $CHCl_3$ (Sigma-Aldrich) in a flask , stirred at room temperature for 30 minutes, then DBU (Fluka), dried over BaO, was added for each mole of the hydroxyl functions. After 1 hour of polymerization reaction, the viscous solution was divided in three different flasks to carry out three different quenching methods. In a flask (a), acetic acid was added to the reaction medium, in an amount equal to that of DBU, to quench the polymerization. Liquid-liquid extraction was carried out on the second flask (b), using slightly acid water solution (0.1M) as aqueous phase to quench the polymerization. Equivalent amount of dried ion-exchange resin Amberlyst® 15, in hydrogen form (Fluka), was added into the third flask (c) and stirred for 2 hours, in order to quench the polymerization. Then, the ion-exchange resin was removed by filtering the solution. The final products (CL30B-g-PLLA-a, b and c) were recovered after drop-by-drop precipitation in 8 volumes of n-heptane, filtered and dried in vacuum overnight at 55°C.

Finally, in order to produce the enantiomeric nanohybrids designed with the 10 wt % in inorganic content (CL30B-g-PLLA and CL30B-g-PDLA), for the further melt-processing, ROP synthesis of the two enantiomeric forms of lactide were carried out using the same synthetic procedure (D-lactide supplied by Purac), quenched by the ion-exchange resin (the reasons will be discussed in the following section).

The properties of the nanohybrids, the effectiveness of the grafting and the DBU removal were assessed by thermal characterization (Differential Scanning Calorimetry, DSC, and Thermogravimetric Analyses, TGA) and Attenuated Total Reflectance Fourier transform infrared (ATR-FTIR) of the dried synthetic products or their fractions recovered after Soxlet extraction from dichloromethane (Sigma-Aldrich). Gel Permeation Chromatography (GPC) was performed in

CHCl3 at 35°C using a Polymer Laboratories liquid chromatograph equipped with a PL-DG802 degasser, an isocratic HPLC pump LC 1120 (flow rate = 1 ml/min) refractive index (ERMA 7517), an automatic injector (Polymer Laboratories GPC-RI/UV) and three columns: a PL gel 10 μm guard column and two PL gel Mixed-B 10μm columns. PS standards were used for calibration. It is worth noting that Gel Permeation Chromatography (GPC) characterization was performed on the soluble fraction recovered after Soxhlet extraction from dicloromethane of both nanohybrids, in order to assess the molecular weight of the nanohybrids synthetized.

Melt Processing

PLA layered silicate composites and references, were prepared by melt-blending using a DSM microcompounder operating at 190°C for 10 min with a rotation speed of 60 rpm. The nanocomposites were elaborated using a commercial PLA (PLA 4032, 4% D-isomer, Naturework) at an inorganic content of 5 wt %, to further improve the inorganic content in the composition compared to the similar systems previously reported (*23*, *29*, *30*). For the sake of comparison, the stereocomplex CL30B-g-PLLA/CL30B-g-PDLA was prepared together with the corresponding reference PLA/CL30B (10 wt % of inorganic content) (see Table 1). To blend stereocomplexes (PLA/CL30B-g-PDLA and CL30B-g-PLLA/CL30B-g-PDLA blends), the temperature was increased to 220 °C for the last 2 min residence time. Inorganic content, thermal properties and thermal stability of blends were assessed using TGA and DSC techniques.

Table 1. Compositions of Composites Produced, by DSM Micro-Compounder

SAMPLE	*PLA [g]*	*CL30B [g]*	*Cl30B-g-PDLA [g]*	*Cl30B-g-PLLA [g]*	*Inorg. content [%]*
PLA 4032 (4% D-isomer)	15	-	-	-	-
PLA/Cl30B 5% inorg.	14	1	-	-	4.8*
PLA/Cl30B 10% inorg.	13	2	-	-	10.4*
PLA/Cl30B-g-PLLA 5% inorg.	7.5	-	-	7.5	5.6*
PLA/Cl30B-g-PDLA 5% inorg.	7.5	-	7.5	-	4.7*
Cl30B-g-PLLA/Cl30B-g-PDLA 10% inorg.	-	-	7.5	7.5	10.5*

* Percentages estimated referring to inorganic content detected by TGA.

In Situ Intercalative Ring-Opening Polymerization of L(D)-lactide

In order to enhance the affinity between nanofillers and the matrix, the CL30B nanofillers were employed to carry out a "grafting from" approach as reported in our previous work (*23*). This consisted to promote ring-opening polymerization (ROP) of L and D-lactide from hydroxyl moieties of quaternary ammonium available at the surface of the organomodified clay in order to synthesize CL30B-grafted bio-nanohybrids, as shown in Figure 1. To promote ROP of L(D)-lactide monomers, 1,8-Diazabicyclo [5,4,0] undec-7-ene (DBU) was employed as metal-free catalysts in chloroform at room temperature. In this respect, two enantiomeric CL30B-g-PLLA and CL30B-g-PDLA nanohybrids were prepared by respective DBU–catalyzed ring opening polymerization (ROP) of L-lactide or D-lactide initiated from the hydroxyl moieties of quaternary ammonium tallow intercalated in the galleries of CL30B (Figure 1).
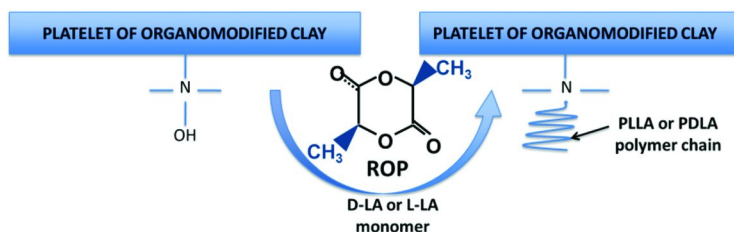

Figure 1. Illustration of the in situ polymerization of polylactic acid chains on Cloisite30B surface.

These nanohybrids were designed at an inorganic content of 10 wt % and confirmed by TGA.

In order to optimize the reaction parameters, especially concerning the selection of the quenching technique, a synthesis just of the L-form of lactide grafted on the clay surface was previously carried out. From the unique reaction solution, three different quenching techniques were performed and the thermal properties of the three different products (CL30B-g-PLLA-a, b and c) were assessed by DSC as well as the effectiveness of the catalyst by FTIR. In particular, the polymerization was quenched by three following approaches, i.e., (a) by adding acetic acid into reaction medium, (b) by liquid-liquid extraction and (c) in the presence of ion-exchange resin. These methods were followed by the selective precipitation of reaction medium into an excess of heptane.

In order to detect the presence of residual catalyst, which can cause degradation during further melt-processing, as previously reported in literature (*28*), Figures 2 and 3 show the respective ATR-FTIR spectra of the DBU, acetic acid and the corresponding salt and those of CL30B-g-PLLA nanohybrids. In Figure 2, the results obtained from spectroscopic analysis indicate that the bands of the DBU salt form, derived from reaction of DBU with acetic acid, are the C-H stretching vibration bands at 2925 and 2854 cm^{-1}, and stretching vibration bands

ν(C=N) at 1643 and 1554 cm⁻¹. As it is possible to observe, comparing Figures 2 and 3, any significant evidence of DBU traces is observed in the case of the nanohybrids, suggesting that all the precipitation techniques adopted are suitable to obtain DBU-free PLLA.

In Figure 3 the spectroscopic results of the products indeed show typical peaks of PLLA. In particular, C=O stretching band at ~1760 cm⁻¹, C-O stretching band at ~1189, 1134 and 1091 cm⁻¹, CH₃ bending vibration at ~1457 cm⁻¹ and C-H bending vibrations at 1382-1370 cm⁻¹, confirming that the polymerization of PLLA was successful. The spectra of CL30B-g-PLLA-c show the slight shifted peaks compared to the CL30B-g-PLLA-a and b suggest that the treatment with the ion-exchange resin has modified both C=O and C-O stretching vibration bands.
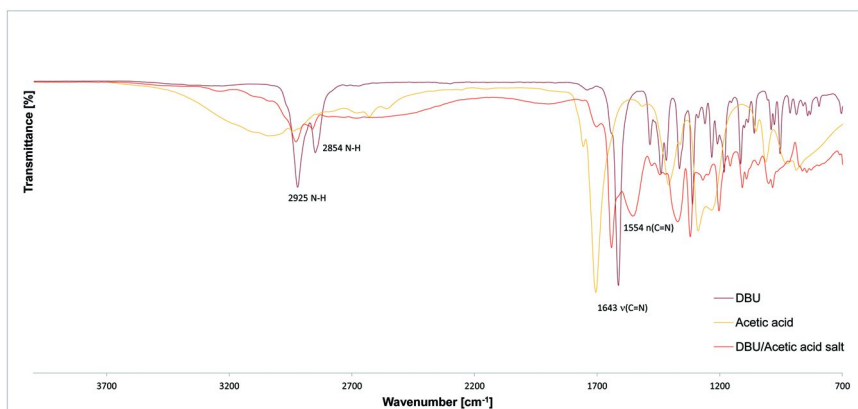

Figure 2. ATR-FTIR spectra of DBU, acetic acid and DBU/acetic acid solution.
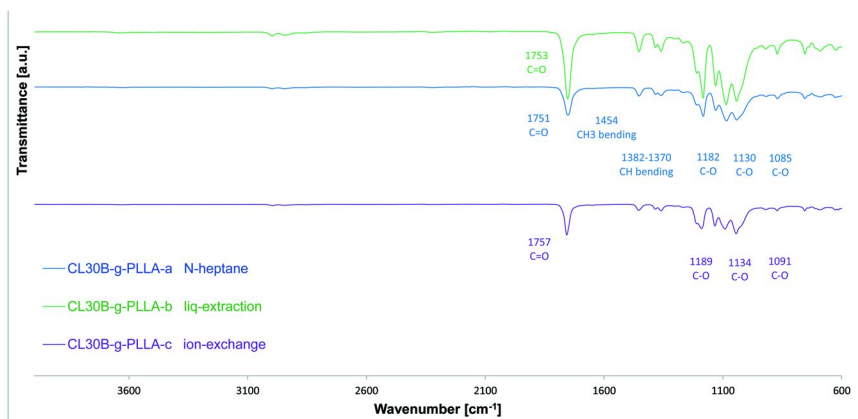

Figure 3. ATR-FTIR spectra of the insoluble fractions recovered after Soxhlet extraction from dichloromethane of different synthetic products (normalized using the peak at 1760 cm⁻¹).

293

To further confirm the thermostability of the nanohybrids, DSC measurements of the different CL30B-g-PLLAs were carried out. DSC measurements have shown to be an efficient way to evidence side-reactions, namely racemization of PLA-based materials on heating (*23*). In Figure 4, DSC thermograms corresponding to the second heating of different extracted products (CL30B-g-PLLA-a, b and c) are reported. In Table 2, the main results of DSC analysis were summarized.

Table 2. Values of the Glass Transition (T_g), Melting (T_m) Temperatures and Heat of Crystallization (ΔH_m) under Nitrogen Flow (Temperature Range: -80-200 °C, Heating and Cooling Rate 10°C /min, Second Heating)

DSC	T_g [°C]	T_m [°C]	$\Delta H_m [J/g]$
CL30B-g-PLLA-a	50.6	160.9	36.2
CL30B-g-PLLA-b	47.5	159.2	37.0
CL30B-g-PLLA-c	54.9	162.0	34.1

Distinguishable T_g temperatures can be identified in the DSC traces. All results can be likely ascribed to PLA of low molecular length (as expected for the designed polymerization).
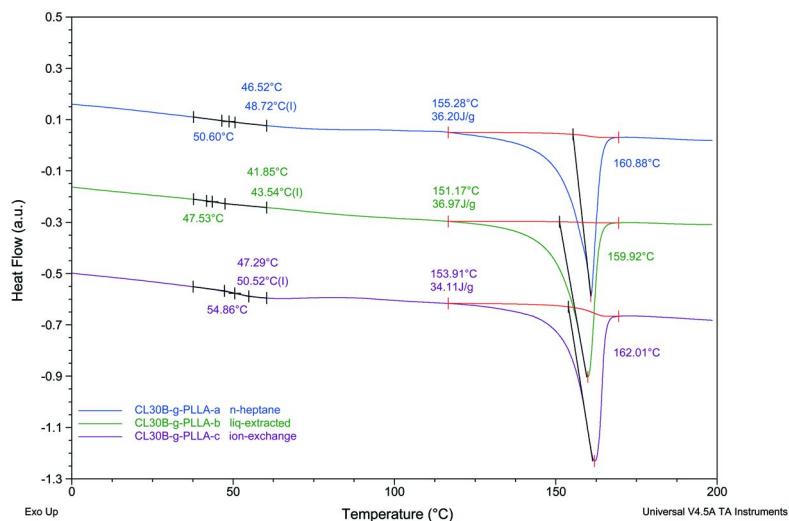

Figure 4. DSC of CL30B-g-PLLA products recovered upon these three quenching techniques.

All the thermal properties recorded for the nanohybrids are typical for a PLLA of low molecular weight, as reported in previous works (*23*, *28*). The CL30B-g-PLLA-a thermogram shows a T_g of around 50.6 °C, a T_m of around 160.9 °C and 36.2 J/g for the crystallization enthalpy. The CL30B-g-PLLA-b shows the slightly lower values of T_g and T_m, and not significant increase in the ΔH_m, compared to the CL30B-g-PLLA-a. The higher values of T_g and T_m were shown by the CL30B-g-PLLA-c product, suggesting the good effectiveness of the third quenching technique. This was further supported after carrying out 10-scan DSC measurements on those nanohybrids. After the second scan, the nanohybrids extracted from the methods (a) and (b) did not exhibit any melting and crystallization features. This indicates that DBU residues could further promote the undesirable transesterification reactions (not shown here). In contrast when ion-exchange resin is employed, the resulting nanohybrids are thermally stable. Taking in account these results, a new series of nanohybrids, two enantiomeric nanohybrids were synthetized using the same procedure and quenching the ROP by the ion-exchange resin approach.

Gel Permeation Chromatography (GPC) characterization (performed in CHCl$_3$ at 35°C) was performed on the soluble fraction recovered after Soxhlet extraction from dicloromethane of both nanohybrids, in order to assess the molecular weight of the nanohybrids synthetized. In Table 3 number-average molecular weight (M_n), the molecular weight at the maximum peak (M_p) and dispersity (DPI) are reported upon a PS calibration.

Table 3. M_n, M_p and DPI of Different Soluble Fractions PDLA and PLLA, Recovered after Soxhlet Extraction from CH$_2$Cl$_2$ of the Corresponding Nanohybrids Cl30B-*g*-PDLA and Cl30B-*g*-PLLA

SAMPLE	M_n *[g/mol]*	M_P *[g/mol]*	*DPI*
PDLA from Cl30B-*g*-PDLA	2.40 x 10^4	4.68 x 10^4	2.1
PLLA from Cl30B-*g*-PLLA	2.50 x 10^4	4.86 x 10^4	2.1

Although we may not exclude any fractionation of these samples from CH$_2$Cl$_2$, these results show that the soluble fraction issued from both nanohybrids have the same range of molecular weights. These results are further confirmed on the basis of thermal properties recorded for both nanohybrids.

To further confirm the previous results, 10-cycles DSC analysis was carried out also on the Cl30B-g-PLLA and CL30B-g-PDLA nanohybrids. As shown in Figure 5, both nanohybrids show a very significant thermostability because the main thermal properties do not change even after 10-cycles heating-cooling scans. This result confirms the effectiveness of the catalyst removal because no evidence of degradations is visible in the thermograms. The enantiomers, at 10% inorganic content, have comparable thermal properties, as shown by their respective glass transition (T_g), melting (T_m) and cold crystallization temperatures (T_c) in Figure 5. The slightly shifted values in the melting temperatures recorded, compared to

the previous results of the CL30B-g-PLLA-a b and c nanohybrids, are expected because the higher inorganic content designed for the two enantiomers CL30B-g-PLLA and CL30B-g-PDLA. In addition, they have two T_m, *that is*, ascribed to the melting and recrystallization events on heating, fairly common in low M_n polylactides or which can be attributed to a polymorphism of the two different crystal forms of polymorphic PL(D)LA (α- and α′-form crystals) (*23*).
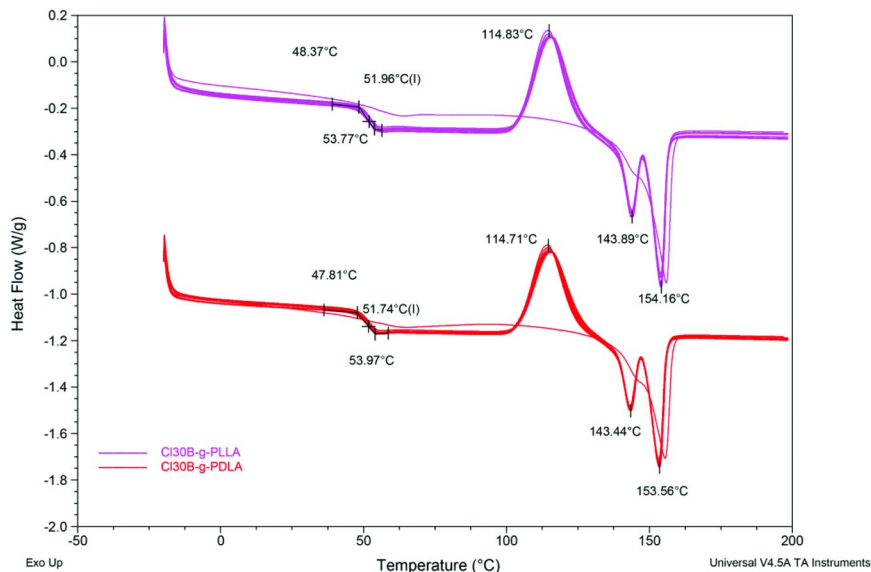

Figure 5. 10-cycles DSC scans of CL30B-g-PDLA and CL30B-g-PLLA (10 wt% of inorganic content).

In this respect, among the different quenching techniques, the ion-exchange resin approach was selected to prepare CL30B-graft-PLLA and CL30B-graft-PDLA nanohybrids thermally stable.

PLA Nanocomposites by Melt Intercalation

To further attest for the efficiency of the quenching ion-exchange resin method, those nanohydrids were subsequently melt-blended with commercial PLA using a DSM microcompounder in order to produce PLA/clay-based bio-nanocomposites. It is worth noting that well-dispersion of nanohybrids into resulting bionanocomposites could be readily achieved and demonstrated by both WAXS and TEM analyses as reported by us (*23*).

A series of DSC experiments was conducted to investigate the thermal properties of the nanocomposites. These DSC results are also compared with those of nanocomposites directly prepared from C30B nanofiller and commercial PLA. Figure 6 shows the first heating scans of nanocomposites and the main results are summarized in Table 4.
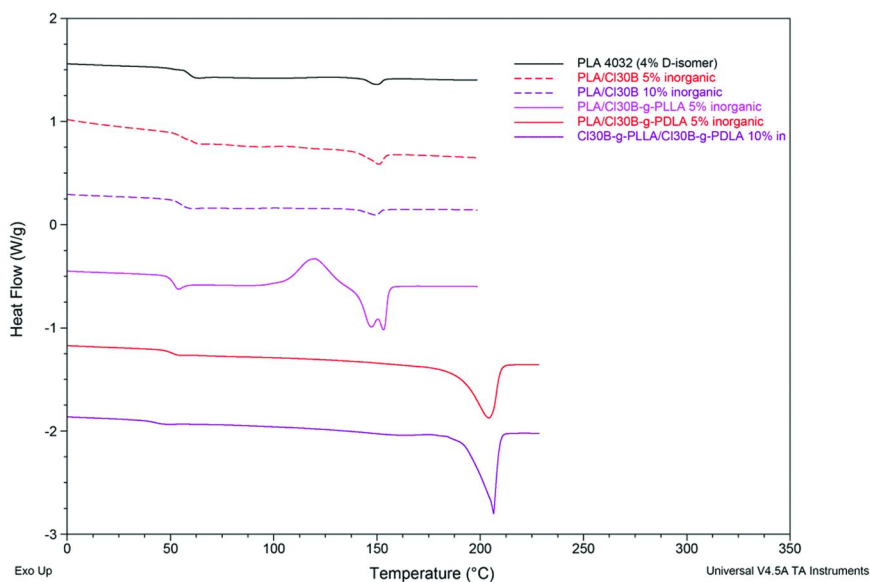
Figure 6. DSC thermograms of the first heating scan of the neat PLA and all the nanocomposites prepared.

The pure PLA matrix contains a low quantity of D-isomer (4%) and exhibits a T_g of around 59°C and an endothermic melting with a melting temperature (T_m) at 150°C. No significant differences were observed in the thermograms of both PLA/CL30B composites, suggesting that the low content of clay in the blend does not affect the thermal properties of the neat PLA. A slight decrease in the T_g suggests the plasticizer effect of the nanohybrids in the blends, likewise due to the low molecular weight of the PL(D)LA chains grafted on the nanoclay surface. The DSC results for the stereocomplex obtained by melt-blending CL30B-*g*-PLLA and CL30B-g-PDLA confirm that the as-grafted polymers are characterized by a lower glass transition temperature, compared to the commercial PLA. The thermograms of both stereocomplexes PLA/CL30B-g-PDLA and CL30B-*g*-PLLA/CL30B-*g*-PDLA interestingly exhibit a comparable melting temperature peak at 205°C, which is above 50°C, compared to the starting nanohybrids (T_m=154°C, see Figure 5) as well as the neat PLA (T_m=150°C, see Figure 6 and Table 4).

The thermal stability of the stereocomplex is also studied by the 10 heating/cooling/heating cycles DSC, reported for both stereocomplex in Figure 7. Their main results are shown in Figs. 8 and 9.

Table 4. Values of the Glass Transition (T_g), Cold Crystallization (T_{cc}), Melting (T_m) Temperatures and Cold Crystallization and Melting Enthalpies (ΔH_{cc} and ΔH_m) Recorded from the First Heating Scan, under Nitrogen Flow (Temperature Range: -20 - 230°C, Heating Rate 10°C /min)

DSC	T_g [°C]	T_{cc} [°C]	ΔH_{cc} [°C]	T_m [°C]	ΔH_m [J/g]
PLA 4032 (4% D-isomer)	59.1	-	-	150.1	3
PLA/Cl30B 5% inorganic	60.6	-	-	150.7	5
PLA/Cl30B 10% inorganic	58.9	-	-	149.4	3
PLA/Cl30B-g-PLLA 5% inorganic	52.1	120.0	26	147.5-153.1	30
PLA/Cl30B-g-PDLA 5% inorganic	51.4	-	-	204.9	46
Cl30B-g-PLLA/Cl30B-g-PDLA 10% inorganic	42.5	-	-	205.4	45

These results confirm the high thermal stability of the stereocomplexes prepared by melt-blending. The melting enthalpies (Figure 9), as well as the melting temperatures (Figure 8), show the stable values (of ~40 J/g and ~200°C, respectively) for both stereocomplexes. For the PLA/Cl30B-g-PDLA stereocomplex, the cold crystallization temperature (T_{cc}) slightly decreases from 106 to 102°C by increasing the heating cycle number. In the case of the direct blend between the synthetic nanohybrids Cl30B-g-PLLA/Cl30B-g-PDLA, the cold crystallization appears after the fifth cycle, characterized by a T_{cc} of 84-85 °C and an enthalpy from 3 to 12 J/g, which increases with the heating cycle number and suggesting that the Cl30B-g-PLLA/Cl30B-g-PDLA is slightly less thermostable than the commercial PLA-based stereocomplex. It is worth noting that no evidence of further melting peaks is observed on the 10 cycle scans, Figure 7, also in the case of the stereocomplex PLA/Cl30B-g-PDLA. It is worth noting that no peaks in the temperature range of the PLA homocrystals (~150°C, see Figure 7) appears, suggesting that the full stereocomplexation of the enantiomers is achieved. This result confirms the possibility by direct melt blending to get full stereocomplexation, being considered as a significant challenge in the melt-preparation of PLA stereocomplexes (*31, 32*).

The stereocomplexation approach, therefore, enables to improve the thermal properties of the nanocomposites. Moreover, for both stereocomplexed nanocomposites, there is no "cold" crystallization, suggesting a significant improvement in the crystallinity rate, as shown in Figures 7 and 9.
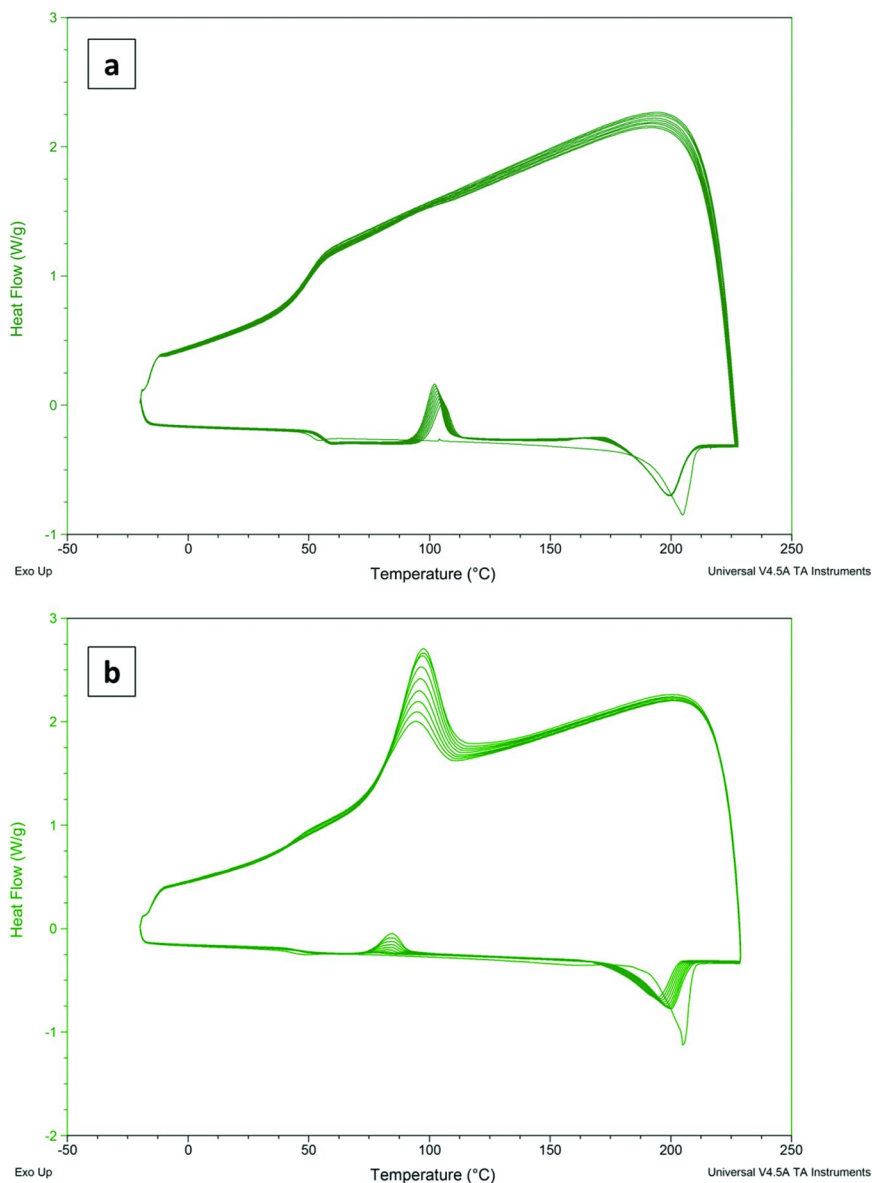
*Figure 7. 10-cycles DSC heating/cooling scans under nitrogen flow
(temperature range: -20-230 °C, heating rate 10°C /min), for the stereocomplex
PLA/Cl30B-g-PDLA (5% inorganic), (a), and Cl30B-g-PLLA/Cl30B-g-PDLA
(10% inorganic), (b).*

	I	II	III	IV	V	VI	VII	VIII	IX	X
Tm (h)	205	200	200	199	198	198	197	196	195	195
Tcc (h)						84	84	84	85	85
Tm (g)	205	199	199	199	199	199	199	199	199	199
Tcc (g)		106	105	105	104	104	103	103	103	102

Figure 8. Values of cold crystallization (T_{cc}) and melting (T_m) temperatures as a function of the heating cycle number (indicated with roman numerals on the top line of the summarizing table under the curve), recorded from the ten cycles DSC thermograms, under nitrogen flow (temperature range: -20-230 °C, heating rate 10°C /min), for the stereocomplex PLA/Cl30B-g-PDLA (5% inorganic, red curves) and Cl30B-g-PLLA/Cl30B-g-PDLA (10%inorganic, violet curves).

	I	II	III	IV	V	VI	VII	VIII	IX	X
DHm (h)	46	38	41	40	41	40	41	39	40	40
DHcc (h)					3	5	7	10	12	
DHm (g)	45	42	42	42	42	43	43	42	42	42
DHcc (g)		17	18	17	18	20	20	20	21	22

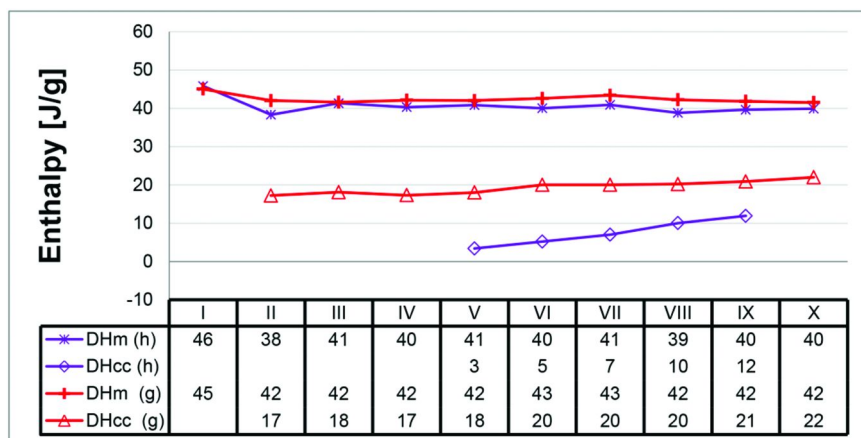*Figure 9. Values of cold crystallization and melting enthalpies (ΔH_{cc} and ΔH_m) as a function of the heating cycle number (indicated with roman numerals on the top line of the summarizing table under the curve), recorded from the ten cycles DSC thermograms, under nitrogen flow (temperature range: -20-230 °C, heating rate 10°C /min), for the stereocomplex PLA/Cl30B-g-PDLA (5% inorganic) and Cl30B-g-PLLA/Cl30B-g-PDLA (10 %-wt inorganic).*

Conclusions

Well-defined and thermally stable Cl30B-g-PLLA (B150-L) and Cl30B-g-PDLA (B150-D) nanohybrids were prepared by DBU–catalyzed ring opening polymerization (ROP) of L-lactide and D-lactide respectively initiated from the hydroxyl moieties of quaternary ammonium cations intercalated in the galleries of Cl30B. Quenching method based on ion-exchange resins led to the preparation of thermally stable nanohybrids. As a result, the bionanocomposites obtained after melt-blending of nanohybrids with PLA were thermally stable, confirming by the full deactivation of metal-free DBU catalyst before melt-processing, overcoming the intrinsic limits related to the use of the DBU as organic catalyst in the ROP. Stereocomplexes obtained by direct melt-blending PLA and the D-isomer based nanohybrid, as well as melt-blending L and D-isomer based nanohybrids, present a higher melting temperature above 50°C than that of commercial PLA. Moreover, no evidence for the homocrystals was detected in the ten-cycle scans for both sterocomplex Cl30B-g-PLLA/Cl30B-g-PDLA and PLA/Cl30B-g-PDLA. The nanocomposites as well the starting nanohybrids show a very significant thermostability proved by their unchanged main thermal properties even after 10- heating/cooling cycles. Furthermore, it was easy to quench the catalyst activity using the ion-exchange resin, enabling to implement these materials into industrial applications.

Acknowledgments

References

1. Kummerer, K. *Green Chem.* **2007**, *9*, 899–907.
2. Jenck, J. F.; Agterberg, F.; Droescher, M. J. *Green Chem.* **2004**, *6*, 544–556.
3. Gross, R. A.; Kalra, B. *Science* **2002**, *297*, 803–807.
4. Kaplan, D. L. *Biopolymer Renewable Resources*; Springer: Heidelberg, 1998; pp 1−29.
5. Lunt, J. *Polym. Degrad. Stab.* **1998**, *59*, 145–152.
6. Raquez, J.-M.; Habibi, Y.; Murariu, M.; Dubois, P. *Progr. Polym. Sci.* **2013**, *38*, 1504–1542.
7. Thomas, C.; Gladysz, J. A. *ACS Catal.* **2014**, *4*, 1134–1138.
8. He, Y.; Xu, Y.; Wei, J.; Fan, Z.; Li, S. *Polymer* **2008**, *49*, 5670–5675.
9. Zhang, J.; Sato, H.; Tsuji, H.; Noda, I.; Ozaki, Y. *Macromolecules* **2005**, *38*, 1822–1828.
10. Anderson, K. S.; Hillmyer, M. A. *Polymer* **2006**, *47*, 2030–2035.
11. Fan, Y.; Nishida, H.; Shirai, Y.; Tokiwa, Y.; Endo, T. *Polym. Degrad. Stab.* **2004**, *86*, 197–208.

12. Alexandre, M.; Dubois, P. *Mater. Sci. Eng.* **2000**, *28*, 1–63.

13. Bordes, P.; Pollet, E.; Avérous, L. Nano-biocomposites: Biodegradable polyester/nanoclay systems. *Progr. Polym. Sci.* **2009**, *34*, 125–155.

14. Chang, J. H.; An, Y. U.; Sur, G. S. Poly (lactic acid) nanocomposites with various organoclays. I. Thermomechanical properties, morphology, and gas permeability. *J. Polym. Sci., Part B: Polym. Phys.* **2002**, *41*, 94–103.

15. Ray, S. S.; Yamada, K.; Okamoto, M.; Ogami, A.; Ueda, K. New polylactide/layered silicate nanocomposites. 3. High-performance biodegradable materials. *Chem. Mater.* **2003**, *15*, 1456–1465.

16. Zenkiewicz, M.; Richert, J. Permeability of polylactide nanocomposite films for water vapour, oxygen and carbon dioxide. *Polym. Test.* **2008**, *27*, 835–840.

17. Zenkiewicz, M.; Richert, J. Effects of nanofillers and sample dimensions on the mechanical properties of injection-molded polylactide nanocomposites. *Polimery (Warsaw, Pol.)* **2008**, *53*, 591–594.

18. Zenkiewicz, M.; Richert, J.; Różański, A. Effect of blow moulding ratio on barrier properties of polylactide nanocomposite films. *Polym. Test.* **2010**, *29*, 251–257.

19. Paul, M.-A.; Alexandre, M.; Degée, P.; Calberg, C.; Jérôme, R.; Dubois, P. Exfoliated Polylactide/Clay Nanocomposites by In-Situ Coordination–Insertion Polymerization. *Macromol. Rapid Commun.* **2003**, *24*, 561–566.

20. Molinaro, S.; Cruz Romero, M.; Boaro, M.; Sensidoni, A.; Lagazio, C.; Morris, M.; Kerry, J. Effect of nanoclay-type and PLA optical purity on the characteristics of PLA-based nanocomposite films. *J. Food Eng.* **2013**, *117*, 113–123.

21. Pluta, M.; Paul, M.-A.; Alexandre, M.; Dubois, P. Plasticized polylactide/ clay nanocomposites. I. The role of filler content and its surface organo-modification on the physico-chemical properties. *J. Polym. Sci., Part B: Polym. Phys.* **2006**, *44*, 299–311.

22. Lepoittevin, B.; Pantoustier, N.; Devalckenaere, M.; Alexandre, M.; Kubies, D.; Calberg, C.; Jérôme, R.; Dubois, P. Poly (ε-caprolactone)/clay nanocomposites by in-situ intercalative polymerization catalyzed by dibutyltin dimethoxide. *Macromolecules* **2002**, *35*, 8385–8390.

23. Lo Re, G.; Benali, S.; Habibi, Y.; Raquez, J.-M.; Dubois, P. *Eur. Polym. J.* **2014**, *54*, 138–150.

24. Thomas, C. M. *Chem. Soc. Rev.* **2010**, *39*, 165–173.

25. Kamber, N. E.; Jeong, W.; Waymouth, R. M.; Pratt, R. C.; Lohmeijer, B. G. G.; Hedrick, J. L. *Chem. Rev.* **2007**, *107*, 5813–5840.

26. Lohmeijer, B. G. G.; Pratt, R. C.; Leibfarth, F.; Logan, J. W.; Long, D. A.; Dove, A. P.; Hedrick, J. L. *Macromolecules* **2006**, *39*, 8574–8583.

27. Dove, A. P. *ACS Macro Lett.* **2012**, *1*, 1409–1412.

28. Coulembier, O.; Moins, S.; Raquez, J. M.; Meyer, F.; Mespouille, L.; Duquesne, E.; Dubois, P. *Polym. Degrad. Stab.* **2011**, *96*, 739–744.

29. Paul, M.-A.; Alexandre, M.; Degée, P.; Calberg, C.; Jérôme, R.; Dubois, P. *Macromol. Rapid Commun.* **2003**, *24*, 561–566.

30. Paul, M-A.; Delcourt, C.; Alexandre, M.; Degée, P.; Monteverde, F.; Rulmont, A.; Dubois, P. *Macromol. Chem. Phys.* **2005**, *206*, 484–498.
31. Tsuji, M. *Macromol. Biosci.* **2005**, *5*, 569–597.
32. Ikada, Y.; Jamshidi, K.; Tsuji, H.; Hyon, S.-H. *Macromolecules* **1987**, *20*, 904–906.